

PAPER • OPEN ACCESS

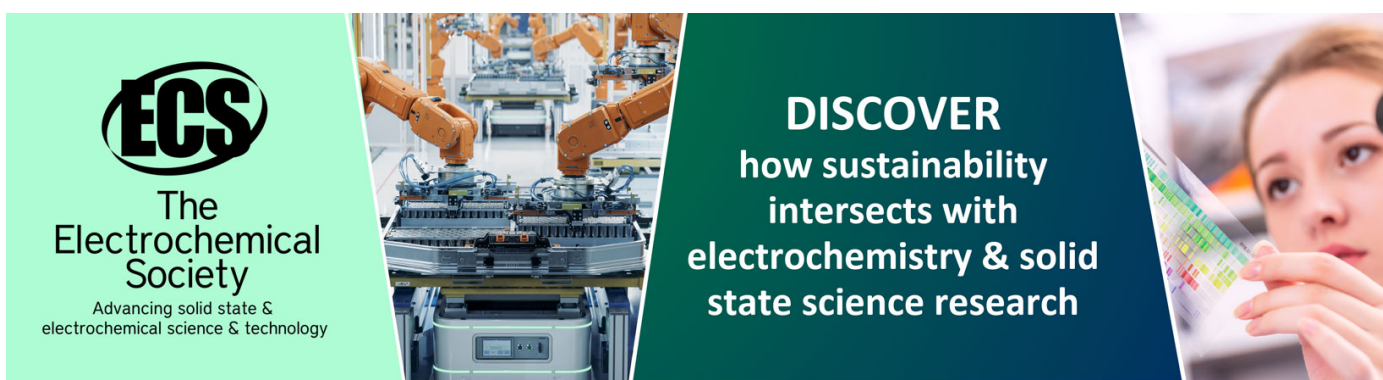
Austenite – ferrite transformation temperature regression equations for low carbon steels with cooling rate account

To cite this article: P. Záhumenský *et al* 2017 *IOP Conf. Ser.: Mater. Sci. Eng.* **283** 012024

View the [article online](#) for updates and enhancements.

You may also like

- [High-throughput characterization phase transformation temperature based on end-quenching methodology](#)
Sihua Luo, Zaiwang Huang, Ziwei Xie et al.
- [New chromium steel grade for creep applications](#)
Lorena M Callejo, José Ignacio Barbero, Mónica Serna-Ruiz et al.
- [Electrochemical Dilatometry of Si-Bearing Electrodes: Dimensional Changes and Experiment Design](#)
Andressa Y. R. Prado, Marco-Tulio F. Rodrigues, Stephen E. Trask et al.



The banner features the ECS logo on the left, a central image of a robotic arm in a factory, and a woman on the right. The text on the banner reads: "DISCOVER how sustainability intersects with electrochemistry & solid state science research". Below the ECS logo, it says "The Electrochemical Society" and "Advancing solid state & electrochemical science & technology".

Austenite – ferrite transformation temperature regression equations for low carbon steels with cooling rate account

P. Záhumský, I. Kohútek* and J. Semeňák

U. S. Steel Košice, 044 54 Košice, Slovak Republic

*Corresponding author: ikohutek@sk.uss.com

Abstract. The austenite-ferrite transformation temperatures evaluated by dilatometry using thermo-mechanical simulator Gleeble 1500D are investigated in this paper. The effect of cooling rates 1, 5, 10 and 15 °C/s on the upper and lower critical transformation temperatures was evaluated for 30 specimens of six material groups. Considering the cooling rate from dilatometry tests and chemical composition ($C \leq 0.2\%$, $Mn \leq 2\%$, $Si \leq 0.26\%$) of particular specimens, the regression equations for both transformation temperatures were derived. These relations have to be satisfied to avoid the crack formation during continuous casting, as well as to provide the hot rolling control. The proposed regression equations are compared with 32 similar ones adopted from 1961 to 2017 and exhibit a good conformity and accuracy.

1. Introduction

For the improvement of the surface quality of continuously cast steels, it is important to study the hot ductility behavior of steels considering their solidifying thermal history along with crack formation during casting. It has been reported [9] that there exist three temperature regions where typical embrittlement is observed in the carbon steels, i.e., drop from the melting temperature (T_m) to 1200 °C (I), decrease from 1200 to 900 °C (II), and cooling from 900 to 600 °C (III). The cause of embrittlement in region (I) is the existence of residual liquid film along the dendritic interfaces. The ductility was found to be independent of the strain rate. In region (II), the precipitation of finely distributed oxy-sulfides at the austenite grain boundary weakens the boundary strength, and therefore such treatments as slow cooling, holding for certain time, or low-rate straining should be used to improve the ductility. On the other hand, the embrittlement in region (III) is manifested by a lower rate of straining. Controlling factors of this embrittlement are grain boundary sliding and the localization of strain to the pro-eutectoid ferrite film along the austenite grain boundary, which is invoked by the $\gamma \rightarrow \alpha$ (austenite to ferrite) transformation [3], 5, 10, 11].

The present work provides a tool to calculate the austenite-ferrite transformation temperatures with the account of the effect of chemical composition of low carbon steels.

2. Methods

Using a Gleeble 1500D thermal deformation simulator of physical processes, the temperature range of $\gamma \rightarrow \alpha$ transformation was defined for the steels and four different cooling rates corresponding approximately to those of slabs, transfer bars (i.e., semi-products during hot rolling between roughing mill and finishing mill), and hot rolled sheets. Standard size tensile specimens with dimensions of $\varnothing 10 \times 110$ mm taken from transfer bar were used in the experiment. The specimens were heated with heating rates of 25 °C s^{-1} and 10 °C s^{-1} to 1200 °C and 1250 °C, respectively. The austenitization temperature of 1250 °C with holding time of 30 s was applied before cooling to room temperature by cooling rates of 1, 5, 10, and 15 °C s^{-1} , as shown in figure 1. The temperature range of $\gamma \rightarrow \alpha$



transformation during cooling was identified using dilatometry for the four different cooling rates. Although two methods (intersectional and tangential) were used for estimation of the upper (Ar_1) and lower (Ar_3) critical transformation temperatures in $^{\circ}C$, only the results obtained by the intersectional one were used for the regression curve construction and estimation of transformation temperatures, which are plotted in figure 2. Due to a problem with accurate estimation of transformation temperatures for grades with high Si content (e.g., dynamo, non-oriented electrical steels and/or some HSLA specimens), specimens with $Si > 0.3\%$ were excluded from the analysis. Moreover, Ar_1 values for steels with carbon content below 0.05% were also excluded, since the eutectoid transformation was not considered to occur for such low carbon content.

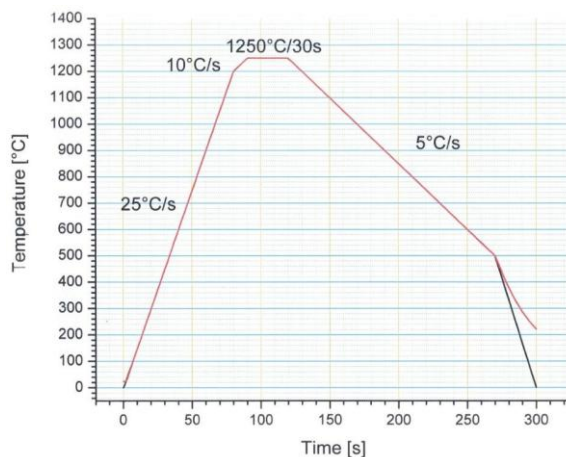


Figure 1. Heating and cooling curves of test specimens by Gleeble equipment

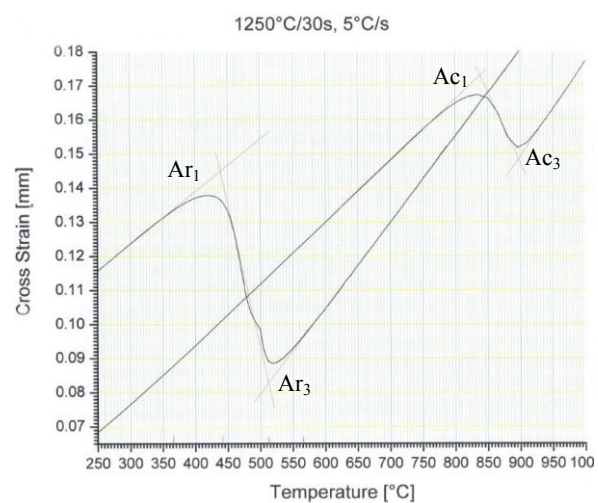


Figure 2. Dilatation curves used for the transformation temperature characterization in the region with a typical embrittlement pattern

The chemical composition of the steels has been determined using a LECO analyzer by Optical Emission Spectral Analysis. Full spectra of 22 chemical elements were measured in total.

3. Material

In total, 30 specimens of 6 material groups were tested, as shown in Table 1.

Table 1. Number of specimens in six evaluated material groups.

Group No	Material group	Short description	Number of specimens
1	C-Mn	C-Mn	9
2	Drawing	Draw	9
3	High-Strength Low-Alloy	HSLA	5
4	Interstitial Free	IF	3
5	Dual-Phase	DP	3
6	Transformation-Induced Plasticity	TRIP	1
Total			30

The contents of C, Mn, and Si (in weight %) for the evaluated materials are depicted in figures 3, 4, and 5, respectively, while the histogram of cooling rates is plotted in figure 6.

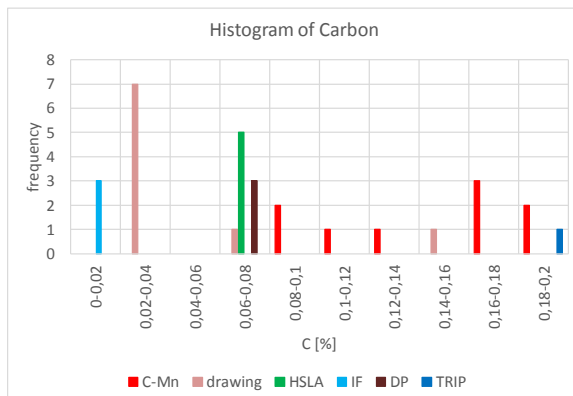


Figure 3. Carbon content in 6 material groups

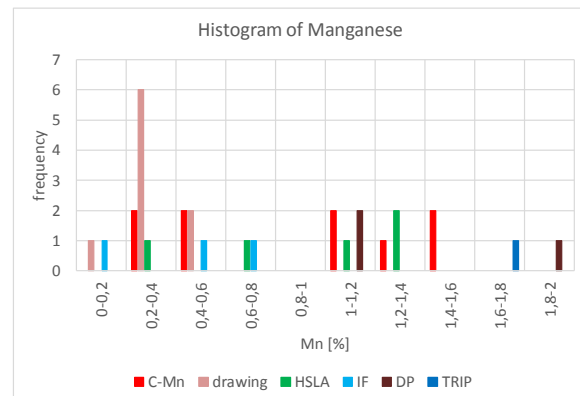


Figure 4. Mn content in 6 material groups

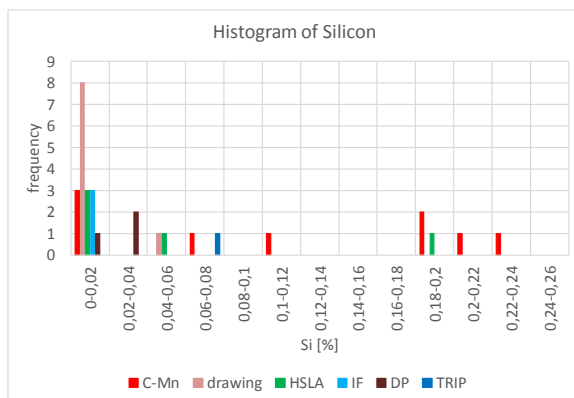


Figure 5. Silicon content in 6 material groups

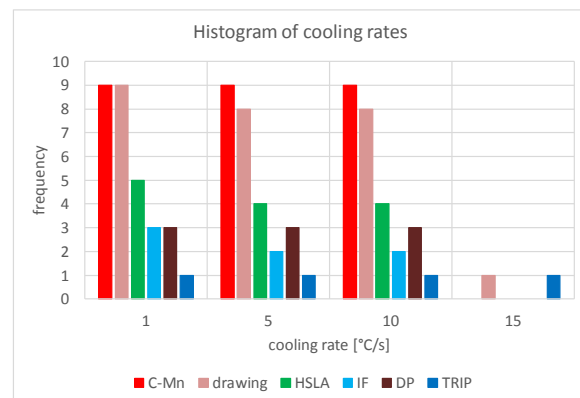


Figure 6. Histogram of cooling rates in 6 groups

4. Results and discussion

The temperature ranges [Ar_3 - Ar_1] of $\gamma \rightarrow \alpha$ transformation during cooling stated by dilatometry for the four different cooling rates via the intersectional method are listed in Table 2.

5. Regression Analysis

Using the measured transformation temperatures Ar_3 and Ar_1 , the respective regression equations were constructed. Each set of independent variables consists of cooling rate as well as content of 22 available chemical elements. Three types of multi-regression were used: stepwise forward (starting with no variables in the model, testing the addition of each variable using a chosen model fit criterion), stepwise backward (starting with all variables, testing the deletion of each variable using a chosen model fit criterion) and regression with fixed set of variables. P-values less than 0.05 of all components were required for all variables in every equation, and correlation between pairs of components were examined to eliminate mutual dependences between chemical elements. Note that in specimens measured in this investigation, an unexpected dependence among Mn, Ti and Nb was discovered, so that only Mn is present in the final equation. Moreover, the distribution of Al content in the set of examined specimens was revealed to be abnormal, and so Al (Al sol) was also excluded from the regression analysis. Thus, although the above elements are very important from the metallurgical point of view, they had to be excluded from the final equations due to statistical reasons.

Final equations are as follows:

$$Ar_3 = +914 - 6.85 \text{ cooling rate} - 650 \text{ C} - 134 \text{ Mn} + 179 \text{ Si} \quad R_{adj}^2 = 0.91 \quad (1)$$

$$Ar_1 = +814 - 9.08 \text{ cooling rate} - 532 \text{ C} - 121 \text{ Mn} + 165 \text{ Si} \quad R_{adj}^2 = 0.90 \quad (2)$$

Table 2. Transformation temperatures of particular grades during cooling

ID	Cooling rate 1 °C s ⁻¹		Cooling rate 5 °C s ⁻¹		Cooling rate 10 °C s ⁻¹		Cooling rate 15 °C s ⁻¹	
	Ar ₃ , °C	Ar ₁ , °C	Ar ₃ , °C	Ar ₁ , °C	Ar ₃ , °C	Ar ₁ , °C	Ar ₃ , °C	Ar ₁ , °C
C-Mn (a)	775	680	725	655	705	635		
C-Mn (b)	650	595	605	520	570	460		
C-Mn (c)	860	735	830	700	660	600		
C-Mn (d)	765	675	780	650	700	625		
C-Mn (e)	815	720	770	675	750	655		
C-Mn (g)	670	630	640	580	620	545		
C-Mn (i)	640	580	605	510	575	475		
C-Mn (j)	650	580	615	530	590	495		
C-Mn (l)	650	595	620	555	600	515		
DP (a)	690	640	660	590	635	555		
DP (b)	710	630	665	595	640	510		
DP (c)	630	560	590	520	570	485		
Draw (a)	845	790	800	740	765	700		
Draw (b)	840	795	815	745	795	720		
Draw (c)	740	620	700	635	685	615		
Draw (d)	835	755						
Draw (e)	835	795	830	750	820	720		
Draw (f)	880	780	870	710	865	690	855	680
Draw (g)	855	800	830	750	805	715		
Draw (h)	840	765	810	710	785	690		
Draw (i)	825	785	780	690	750	670		
HSLA (a)	730	605	660	585	645	520		
HSLA (b)	845	670						
HSLA (c)	775	645	690	630	680	620		
HSLA (d)	725	560	650	595	645	520		
HSLA (e)	770	695	720	610	700	600		
IF (a)	860	835	855	805	845	785		
IF (b)	910	820						
IF (c)	745	715	725	695	720	685		
TRIP	590	550	540	430	460	370	430	370

The comparison of measured temperatures with those estimated via regression equations (1) and/or (2) with an account of chemical composition and cooling rate is shown in Figure 7 (Ar₃) and Figure 8 (Ar₁). Differences between the measured value and that estimated from regression equation are shown in histograms plotted Figure 9 (Ar₃) and Figure 10 (Ar₁).

There are many empirical equations to calculate $\gamma \rightarrow \alpha$ transformation temperatures derived by several authors for special steel grades and special conditions. The most comprehensive list of them is available in [4], other can be found in [1][2], [6][7]. In [9] total, seven equations for Ar₁, as well as 25 equations for Ar₃, are compared with equations (1) and (2). Variables in the mentioned equations are of three types: (a) plain linear variable, (b) combination of two chemical elements (8% of Ar₃ equations, e.g., Si Ni) and (c) non-linear function (54% of Ar₃ equations - e.g. logarithm, exponent, square root) – see Table 3. The coefficient of particular variable in regression equation (only those which are used in more than 1/3 of equations) are shown in real scale in

Figure 11 for Ar₃ and in

Figure 12 for Ar₁: red circle denotes value of coefficients derived for equations (1)-(2) in this paper.

The intercept of all Ar₃ equation is between 810 °C and 914 °C (910 °C is known as A3 for ideal equilibrium iron-carbon binary phase diagram), except for that of Yuan [4] for non-deformed austenite (marked as YN in

Figure 11), which consists mainly from the combination and/or non-linear functions of variables. The intercept used in all Ar₁ – related equations is between 706 °C and 814 °C. The value of 723 °C is referred to as A1 for the ideal equilibrium iron-carbon binary phase diagram.

It is generally adopted that the cooling rate affects the transformation temperature, while increasing the cooling rate decreases transformation temperatures – in equations (1) and (2) increasing cooling rate by $1\text{ }^{\circ}\text{C s}^{-1}$ causes decrease of Ar_1 by $9\text{ }^{\circ}\text{C}$ and/or Ar_3 by $7\text{ }^{\circ}\text{C}$. The cooling rate is included in only approx. 1/7 of equations (probably because transformation temperatures were estimated from the process with a very slow cooling – sometimes they are denoted as Ae_1 and/or Ae_3 , where "e" stands for equilibrium, see [4]).

The coefficients of carbon C, Mn and Ni have the same negative orientation for all equations caused a decrease of transformation temperatures with their increasing contents. The Si coefficients are all positive what is in concordance with expected increasing of transformation temperatures with increasing Si content according to binary Fe-Si diagram. The regression coefficient of chromium (not included in the equations derived in this paper) is mostly negative with 2 exceptions for Ar_3 and positive in all equations for Ar_1 .

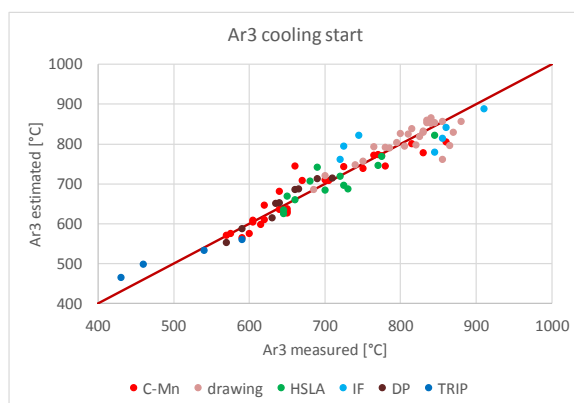


Figure 7. Comparison of measured temperatures Ar_3 with those obtained via equation (1)

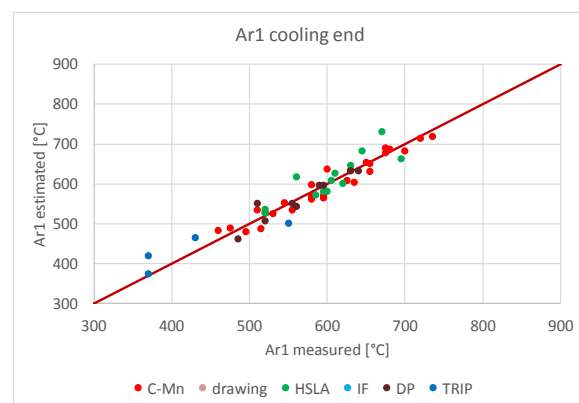


Figure 8. Comparison of measured temperatures Ar_1 with those obtained via equation (2)

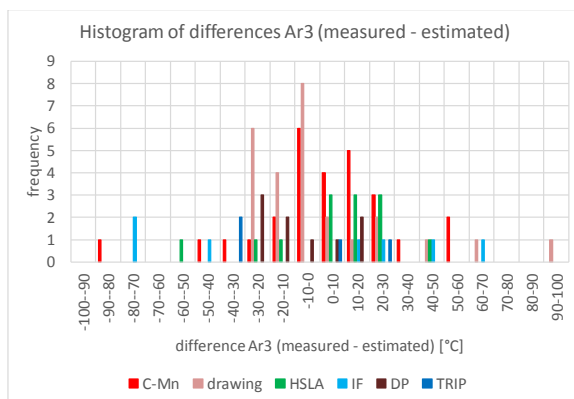


Figure 9. Histogram of differences between measured Ar_3 / Ar_3 and those obtained via regression equation (1)

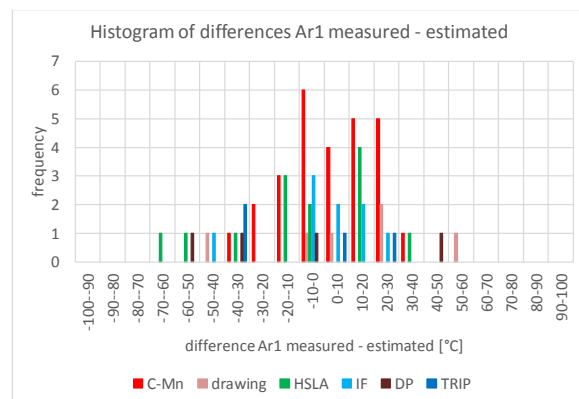
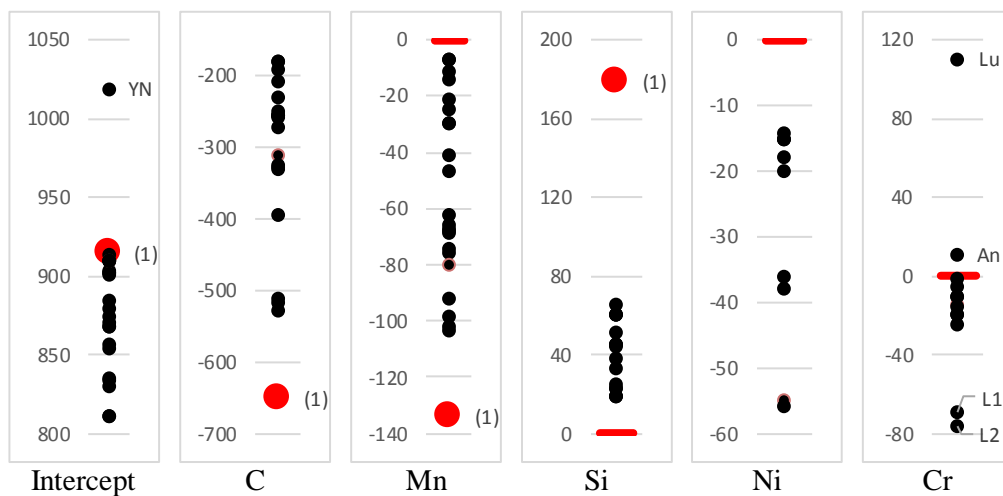


Figure 10. Histogram of differences between measured Ar_3 / Ar_3 and those obtained via regression equation (2)

Given the above discussion, it can be concluded that the obtained results are sufficient for practical purpose of avoiding the crack formation during continuous casting and hot rolling control as well. However, a deeper insight into the embrittlement mechanism requires additional experiments including qualitative and quantitative phase analysis.

Table 3. Number of variables used in the regression by various authors

Variable	Number of equations		Share of equations in the total scope	
	Ar ₁	Ar ₃	Ar ₁ (% from 8)	Ar ₃ (% from 26)
Intercept	8	26	100.0	100.0
Cooling rate	1	4	12.5	15.4
C	5	20	62.5	76.9
Mn	8	23	100.0	88.5
Si	7	18	87.5	69.2
Ti		3	0.0	11.5
Nb		7	0.0	26.9
V	1	5	12.5	19.2
Cu		7	0.0	26.9
Al		3	0.0	11.5
Al_sol			0.0	0.0
Ni	5	10	62.5	38.5
Cr	5	13	62.5	50.0
Mo	2	9	25.0	34.6
P		4	0.0	15.4
W	1	2	12.5	7.7
S		2	0.0	7.7
Zr			0.0	0.0
B		1	0.0	3.8
Ca			0.0	0.0
As	1	1	12.5	3.8
Sn			0.0	0.0
Sb			0.0	0.0
N		1	0.0	3.8
Others – linear combination		2	0.0	7.7
Others – non-linear		14	0.0	53.8

**Figure 11.** Comparison of regression coefficients of various authors for selected variables in regression equation (1) for Ar₃

In figure 11, “An” stands for Andrews [4], L1 and L2 mean Lotter A and Lotter B in [4], respectively, “Lu” stands for Lutsenko in [4], and “YN” refers to the equation of Yuan for non-deformed austenite in [4].

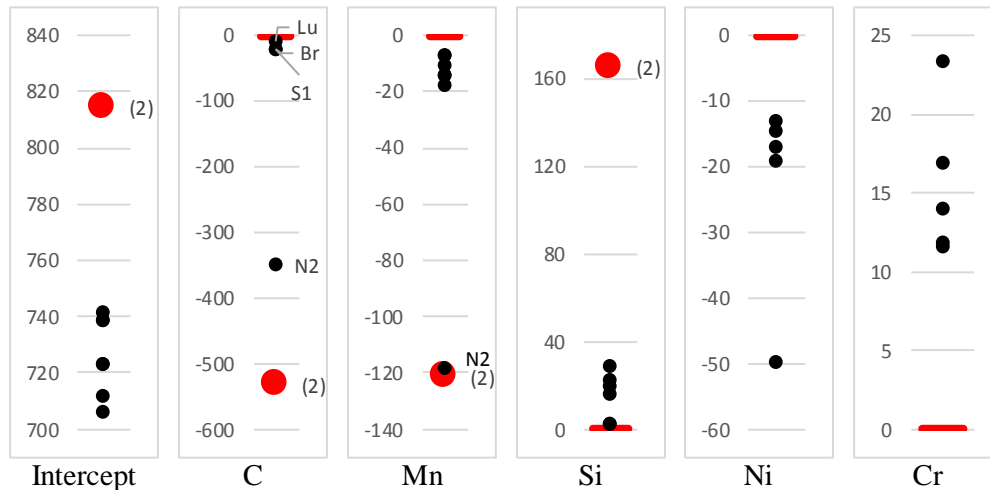


Figure 12. Comparison of regression coefficients of various authors for selected variables in regression equation (2) for Ar1

In f

Figure 12, “Br” refers to Brandis in [4], Lu to Lutsenko in [4], N2 stands for Proprietary 3 in [4] or Nippon 2 in [9], while S1 stands for Schacht in [4].

6. Conclusions

- The experimental material characteristics can be utilized to avoid crack formation during bending and especially at the unbending section below the caster. This way, the surface quality of the final product can be improved.
- The data and regression equations on the austenite-ferrite transformation temperatures are instrumental for the control of process parameters during hot rolling.

Acknowledgment

This study was prepared and published with the support of the research and innovation operational program for the project “Support to Industrial Research and Development Centre in the field of new materials and technologies of coating and welding” (ITMS NFP313011B635), funded from the budget of the European Fund of Regional Development.

References

- [1] Blás J G et al 1989 Influência da composição química e da velocidade de resfriamento sobre o ponto Ar3 em aços de baixo C microligados ao Nb. In: Congresso Anual da Associação Brasileira de Metais, ABM, São Paulo, **1**, pp.11-29.
- [2] Choquet P et al 1985 Mathematical Model for Predictions of Austenite and Ferrite Microstructures in Hot Rolling Processes. IRSID Report, St. Germain-en-Laye, p.7
- [3] Dossett, J L and Boyer H E 2006 Practical Heat Treating, ASM International, 2nd Edition, p.296.
- [4] Gorni A A 2008 Steel Forming and Heat Treatment Handbook, **15**, p.13

- [5] Lee Y K, Hong J M, Choi C S and Lee J K 2005 Continuous cooling transformation temperatures and microstructures of niobium bearing microalloyed steels. *Materials Science Forum*, **475-479**, pp.65-68
- [6] Ouchi C, Sampei T and Kozasu I 1982 The effect of hot rolling condition and chemical composition on the onset temperature of γ - α transformation after hot rolling. *Trans. ISIJ*, pp.214-222
- [7] Pickering F B 1986 Steels: Metallurgical Principles. In: *Encyclopedia of Materials Science and Engineering*, vol. 6, The MIT Press, Cambridge.
- [8] Shiga C et al 1981 Development of Large Diameter High Strength Line Pipes for Low-Temperature Use. Kawasaki Steel Technical Report, Dec. 1981, pp. 97-109
- [9] Staňková H, Motyčka P, Meyer L W and Mašek B 2006 Verification of the validity of the common phenomenological models for low-alloyed trip steel. In: Trends in the Development of Machinery and Associated Technology, 10th International Research/Expert Conference, TMT 2006, Barcelona-Lloret de Mar, Spain, pp. 11-15.
- [10] Suzuki H G, Nishimura S and Yamaguchi S 1982 Characteristics of hot ductility in steels subjected to the melting and solidification *Trans. ISIJ*, **22**, p.48-56.
- [11] Vega M I, Medina S F, Chapa M and Quispe A 1999 determination of critical temperatures (t_{nr} , a_{r3} , a_{r1}) in hot rolling of structural steels with different Ti and N contents. *ISIJ International*, **39**, 12, pp.1304-1310